The Structure of Gemini Surfactant Self-Assemblies Investigated by Energy Dispersive X-ray Diffraction

Giulio Caracciolo,[†] Giovanna Mancini,[‡] Cecilia Bombelli,[†] Paola Luciani,[†] and Ruggero Caminiti*[,†]

Dipartimento di Chimica and INFM, and ICCOM- Sezione di Roma (c/o Dipartimento di Chimica), Università 'La Sapienza', P.le A. Moro 5, 00185 Rome Italy

Received: May 9, 2003; In Final Form: July 30, 2003

Solid-supported multibilayers of the enantiomers of the cationic gemini surfactant **1**, i.e., (2S,3S)-2,3-dimethoxy-1,4-bis(*N*-hexadecyl-*N*,*N*-dimethylammonium)butane dibromide (**1a**) and (2R,3R)-2,3-dimethoxy-1,4-bis(*N*-hexadecyl-*N*,*N*-dimethylammonium)butane dibromide (**1b**), have been studied by means of energy dispersive X-ray diffraction. The effect of substrate on the orientation of the sample has been investigated. Dehydration/hydration kinetics of the samples under enviromental conditions has been followed. Furthermore, we have characterized the structural properties of the meso form, (2S,3R)-2,3-dimethoxy-1,4-bis(*N*-hexadecyl-*N*,*N*-dimethylammonium)butane dibromide (**1c**). The reported results indicate that the spontaneous self-assemblies of the meso form present different physical characteristics.

1. Introduction

Gemini surfactants are a class of surfactants characterized by two polar headgroups, connected by a spacer of various kind, and two hydrophobic tails. This structural feature provides gemini unique properties among the surfactants. Gemini, for example, form aggregates at a concentration almost a 100-fold lower than the corresponding single chain surfactants and even have 1000-fold higher surface activities.[1] By virtue of their unique properties, gemini surfactants represent an interesting topic of study, both for industry[2] and academic research.[1,3] Of particular interest are cationic gemini surfactants and their potential for use in transfection for the high binding and transportation capability of DNA and drugs into living cells.[4] Some of them have been found to display high transfection activities.[4d,e] Considering the many peculiarities of this class of surfactants and because they strictly depend on the nature of the spacer, we have approached the study of a cationic gemini surfactant with stereogenic centers on the spacer, 2,3-dimethoxy-1,4-bis(*N*-hexadecyl-*N*,*N*-dimethylammonium)butane dibromide.[5] The interest in chiral surfactants and their aggregates meets many perspectives. Chiral aggregates have been used as suitable media for enantioselective reactions[6] and separation of chiral substances such as pharmaceuticals.[7] Chiral recognition in self-assemblies is, in general, largely investigated[8] and has been observed by different means in micellar aggregates.[8c,g,h] It is responsible for the differences observed in assemblies formed by either racemic or homochiral surfactants.[8b,d,f] Because most biological lipids are chiral, the origin of chiral recognition in surfactant self-assemblies is of high interest in biochemical fields, as this is one aspect of molecular recognition responsible for cell membrane compartmentalization. Moreover, in many cases enantiomers display different physiological effects, and chiral recognition in self-assemblies is of fundamental interest from two points of view when vesicles are used as drug delivery systems: (i) the stereochemistry of the surfactant itself may play a crucial role as far as interaction with cell membrane and toxicity are concerned; (ii) chiral recognition may yield selective binding of a chiral drug. It must be noted that health and regulatory authorities such as the FDA have defined strict requirements to patent new chiral drugs, demanding a full documentation of the separate pharmacological and pharmacokinetic profiles of the individual enantiomers, as well as their combination.[9]

It is well recognized that most of the achievements reached in gene transfection are based on trial and error, and satisfactory progress in transfection efficiency cannot leave exclude a detailed comprehension of the roles played by all of the physical−chemical properties of surfactants.[10] Among these, the manner in which the molecular structure of surfactants affects the morphology of the aggregates and their biological activity is an important issue that needs to be clarified. Because it is well recognized that a real enhancement of transfection efficiency requires a full understanding of their supramolecular structures,[11] a systematic structural characterization of the spontaneous surfactant self-assemblies should constitute one of the main goals in this field in order to improve the biological performance of these gene delivery vehicles. Here we report an energy dispersive X-ray diffraction (EDXD) study of the enantiomers of the cationic gemini surfactant **1**, i.e., (2S,3S)-2,3-dimethoxy-1,4-bis(*N*-hexadecyl-*N*,*N*-dimethylammonium)-butane dibromide, **1a**, and (2R,3R)-2,3-dimethoxy-1,4-bis(N-hexadecyl-*N*,*N*-dimethylammonium)butane dibromide, **1b**, (Figure 1). Moreover, we characterized the structural features of the meso form, (2S,3R)-2,3-dimethoxy-1,4-bis(*N*-hexadecyl-*N*,*N*-dimethylammonium)butane dibromide, **1c**.

2. Materials and Methods

Surfactant **1** was prepared by quaternization of the proper diastereomer of 2,3-dimethoxy-1,4-bis(*N*,*N*-dimethylamino)-butane with a 20% excess of 1-bromohexadecane in benzene at ambient temperature. The white precipitates were purified and characterized as previously described.[5a]

* Corresponding author. Tel: 0039 06 4991 3661. Fax: 0039 06 490631. E-mail: r.caminiti@caspur.it.
[†] Dipartimento di Chimica and INFM.
[‡] ICCOM−Sezione di Roma.

10.1021/jp035282e CCC: $25.00
Published on Web 10/09/2003

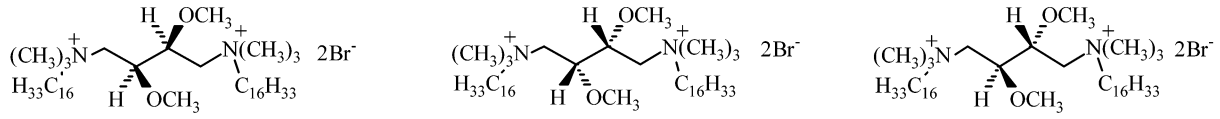

Figure 1. Structure of the studied cationic gemini surfactants: **1a**, **1b**, **1c** (from left to right).

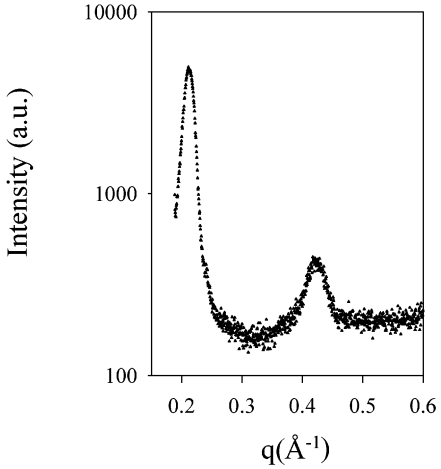

Figure 2. Diffraction pattern of fully hydrated **1a** multilamellar oriented stack. The noticeable sharp reflections are the first- and second-order Bragg peaks, whereas the diffuse scattering is due to the random stacking disorder.

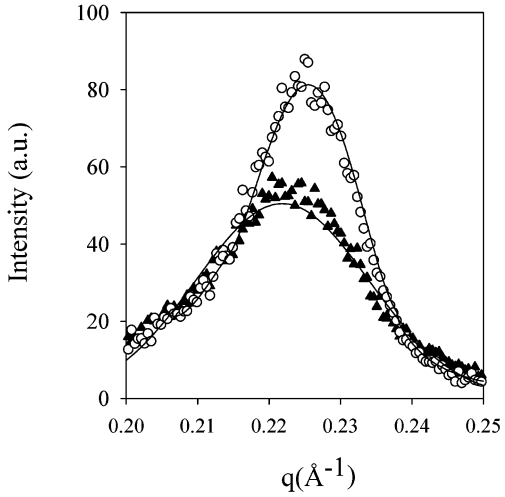

Figure 3. Comparison between the initial (black triangles) and final (open circles) spectra in the dehydration kinetics collected at $\theta = 0.8°$, both fitted by Gaussian distributions (solid lines). The structures appear similar even if differences in the peak position and in their relative amplitude are clearly visible.

Sample Preparation. A 0.012 M aqueous solution of **1** was prepared by adding 1 mL of bidistilled water to 10 mg of surfactant **1** and gently heating until completely dissolved. Oriented samples were prepared by spreading few drops of the lipid solution onto the oriented surface of cleaned silicon wafers and onto a glass-made support. The surfaces were gently fluxed with nitrogen for 8 h and, after evaporation of the solvent, the samples were kept in a vacuum for 12 h to remove any traces of solvent. The lipid films were subsequently hydrated fully from a water-saturated atmosphere. This procedure allows to prepare fully hydrated solid-supported multibilayers.

X-ray Diffraction Experiments. X-ray diffraction experiments were carried out by using an EDXD apparatus elsewhere described.[12a,b,13] An incident polychromatic X-ray radiation was used, and the diffracted beam was energy resolved by a solid-state detector located at a suitable scattering angle θ.

The diffractometer operates in vertical θ/θ geometry and is equipped with an X-ray generator (W target), a collimating system, step motors, and a solid-state detector connected via an electronic chain to a multichannel analyzer. The X-ray source is a standard Seifert tube operating at 50 kV and 40 mA, using Bremsstrahlung radiation, and the detecting system is composed of an EG&G liquid nitrogen cooled ultrapure Ge solid-state detector connected to a PC through ADCAM hardware. Both the X-ray tube and the detector can rotate around a common center where the sample is placed.

The diffracted intensity was normalized to the incident polychromatic radiation and to all the parasitic effects. Background scattering from the substrates was subtracted.

The uncertainty associated with θ is $\Delta\theta = 0.001°$, and it directly affects the uncertainty Δq associated with the transfer momentum q ($q = aE \sin\theta$; $a = 1.01354$ Å^{-1} keV^{-1}).

3. Results and Discussion

Figure 2 shows the diffraction pattern collected at $\theta = 0.8°$ from **1a** multibilayers aligned on a silicon substrate and fully hydrated using water vapor at 100% relative humidity at room temperature. The intensity of diffraction is great from stacks of bilayers because their normal is aligned along the *z*-component of the transfer momentum q_z. Conversely, in the case of multilamellar vesicles, the normal to the bilayers are isotropically distributed in space, giving rise to weak powder-like diffraction patterns whose intensity decreases as $1/q^2$. The main advantages of nonisotropic samples are a plain discrimination between in-plane and out-of-plane structures and a remarkable decrease in the acquisition time.[14] As such, the use of aligned samples is highly auspicious because they present the same physical characteristics as their equivalents immersed in liquid water, especially in view of the recent overcoming of the "vapor pressure paradox" by Katsaras.[15−17] Thus, oriented membrane stacks can realistically be used as useful model systems of biological membranes.

In Figure 2 we observed only two orders of diffraction as usual for the major part of fully hydrated samples, i.e., in excess water, in the fluid L_α phase.[18] From the pattern, a well-defined lamellar periodicity of 28.4 Å was determined using the Bragg relation $D = 2\pi/q$. The position of the diffraction peaks was determined to within an accuracy in D of 0.1 Å by a Gaussian fit to the data. In contrast to the traditional angular dispersive X-ray diffraction (ADXD), EDXD permits the simultaneous acquisition of the spectrum points at each value of q in the investigated range. This peculiar characteristic of the technique allows us to perform kinetic studies.[19] To detect the structural stability and the degree of hydration of the sample under the environmental conditions, a kinetic study was performed by collecting a diffraction pattern every 200 s for an overall period of 40000 s. Structural and dynamical membrane properties can indeed change dramatically with hydration so that full hydration is usually a basic requisite in order to associate experimental findings to the biological state.[20]

In Figure 3 we report the comparison between the initial and the final first-order peaks, both fitted by a Gaussian curve. It is interesting to note that the peaks do not present the same

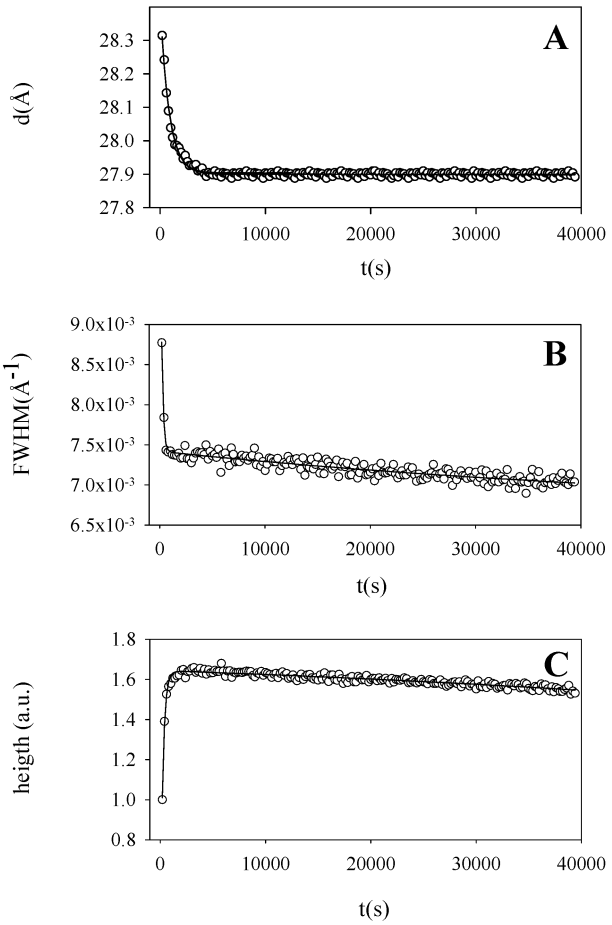

Figure 4. Dehydration kinetics of **1a** as a function of time: the calculated *D*-spacing (panel A), the fwhm (panel B), and the normalized height (panel C) of the first-order diffraction peak.

features, i.e., height, width, and position. Analyzing all the collected spectra, we directly calculated the corresponding *D*-spacings: the starting value of 28.4 Å monotonically decreases as a function of time until the equilibrium condition at 27.9 Å is reached (Figure 4, panel A). In the present study this equilibrium state of the system is considered as reference state. To fit the *D*-spacing time dependency, the follow single-exponential law was used:

$$D(t) = D_F + D_1 \exp(-t/\tau_D) \quad (D_S(t) \geq D_{SF}\, t \in (0, \infty)) \quad (1)$$

where D_F is the *D*-spacing in the reference state, D_1 is the amplitude of the decay, and τ_D is the mean decay time. For $t = 0$, which is the initial point of the kinetics, the equation yields maximum *D*-spacing value. Fitting the experimental data with eq 1, we found time constant value $\tau_D \sim 864$ s^{-1} for dehydration. The degree of hydration of both the initial and final state was evaluated by thermogravimetric measurements which provide the number of waters per lipid, n_w. These measurements gave a thin water layer of 3.5 water molecules per lipid molecule in the fully hydrated state. Each lipid headgroup has a certain number of water molecules attached via hydrogen bonds. The occurred dehydration reduces n_w to 1.5 waters per lipid, thus accounting for the observed reduction of *D*-spacing. The observed reduction can be interpreted in terms of partial dehydration of the sample under the enviromental conditions, which does not affect the structured first hydration shell. At thermodynamic equilibrium, the activity of adsorbed water is the same as the water atmosphere in the sample cell

TABLE 1: Fitting Parameters of the Relaxation Curves of 1a Obtained Using Equations 1−3

fitting parameters	1a
D_F (Å)	27.9
D_1 (Å)	5.4×10^{-1}
τ_{D1} (s^{-1})	8.47×10^{2}
σ_0 (Å^{-1})	6.63×10^{-3}
σ_1 (Å^{-1})	4.97×10^{-3}
σ_2 (Å^{-1})	7.81×10^{-4}
$\tau_{\sigma 1}$ (s^{-1})	1.54×10^{2}
$\tau_{\sigma 2}$ (s^{-1})	5.50×10^{4}
H_0 (a.u.)	1.77
H_1(a.u.)	1.43
H_2 (a.u.)	2.30×10^{-1}
τ_{H1} (s^{-1})	2.45×10^{2}
τ_{H2} (s^{-1})	7×10^{4}

and the *D*-spacing does not vary anymore.[21] This interpretation is also enforced by the evident diminution of the full width at half-maximum (fwhm) of the Gaussian fit to the first-order diffraction peak as a function of time, which reflects a progressive stabilization of the multibilayer structure and a reduction of the "second order−disorder" in the crystal lattice (Figure 4, panel B). Indeed the water molecules have liquid-like disorder and fill the space between membranes producing irregular variations of the repeating distance *D* in the multibilayer stack. Thus dehydration reduces membrane fluctuations and the *D*-spacings distribution.[22] The fwhm is the mosaic spread, i.e., the degree of orientation of the bilayers on the substrate. Indicating fwhm as σ and fitting the profile with the following temporal evolution law

$$\sigma(t) = \sigma_0 + \sigma_1 \exp(-t/\tau_{\sigma 1}) + \sigma_2 \exp(-t/\tau_{\sigma 2}) \quad (\sigma(t) \leq \sigma_0, t \in (0, \infty)) \quad (2)$$

we find $\tau_{\sigma 1} \sim 154$ s^{-1} and $\tau_{\sigma 2} \sim 5.7 \times 10^4$ s^{-1}. In this case a double-exponential model is the best fit to the experimental data. In the same Figure 4 (panel C) we report the normalized first-order peak height as a function of time. Fitting the raw data by the following model:

$$H(t) = H_0 - H_1 \exp(-t/\tau_{H1}) - H_2 \exp(t/\tau_{H2}) \quad (H(t) \geq H_0, t \in (0, \infty)) \quad (3)$$

we find $\tau_{H1} \sim 245$ s^{-1} and $\tau_{H2} \sim 7 \times 10^4$ s^{-1}.

All the fitting parameters are reported in Table 1. Then, the same **1a** sample was additionally dehydrated under a gentle flux of high-purity nitrogen for an overall period of 5 h. Even in this case we investigated the relaxation process of the sample for the same period of time (40000 s), and the comparison between the initial and the final diffraction patterns of extra-dehydrated **1a** collected at $\theta = 2.4°$ is reported in Figure 5.

Upon this extra dehydration, a further reduction of the *D*-spacing up to 27.6 Å was observed. This value is about 0.3 Å lower than that corresponding to the above-reported equilibrium condition. Regardless, even if the starting point of the kinetics refers to a more dehydrated state than that of reference, Figure 5 clearly shows that the equilibrium condition is exactly the same as before.

Indeed, the uptake of water allowed the lipid film to restore the same hydration shell, resulting in the increase of the *D*-spacing up to the final equilibrium value of 27.9 Å. On hydration, water was taken up from the enviroment resulting in a reversible behavior. This finding confirm that the reference state is effectively the thermodynamic equilibrium condition of the system, as expected in view of the fact that the chemical

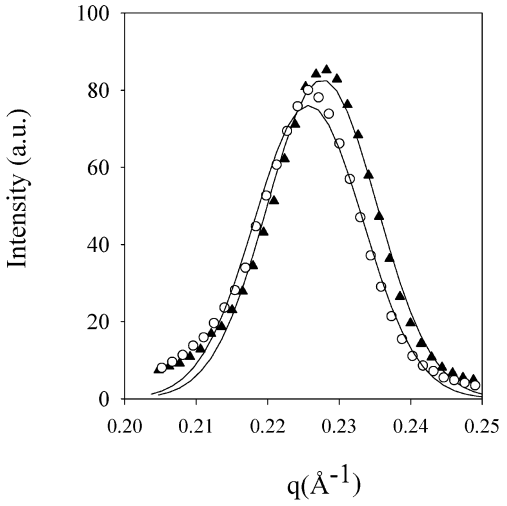

Figure 5. Comparison between the initial (black triangles) and final (open circles) spectra after hydration collected at $\theta = 2.4°$ (for details see the text). The solid line is the best Gaussian fit to the data.

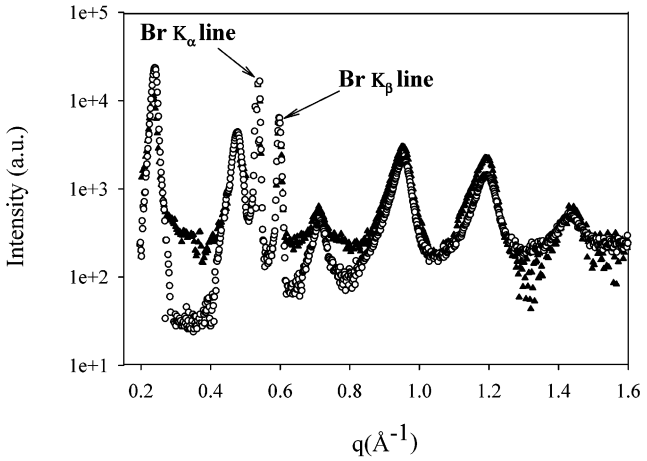

Figure 6. EDXD pattern of **1a**: black circles indicate glass substrate and open circles indicate the silicon substrate. We only show data up to $q = 1.6$ Å^{-1}. For higher q values the diffracted intensity remains constant.

potentials of liquid water and water vapor in equilibrium are exactly the same. The only difference between the final spectra reported in Figures 3 and 5 is due to a different q resolution, which depends on the employment of different diffraction angles. The time constants for dehydration and hydration kinetics are almost the same (hydration data not reported). Subsequently, the effect of the substrate on the mosaic spread of the sample was investigated by aligning **1a** multibilayers onto smooth silicon and rough glass substrates. The samples were partly dehydrated in order improve the experimental resolution of structural data. A suitable diffraction angle $\theta = 2.4°$ was chosen to cover a wide q range between 0.18 and 2 Å^{-1}, enabling the simultaneous collection of multiple Bragg reflections (Figure 6). The lamellar D-spacing of 27.9 Å, calculated as above explained, ensures that the system is effectively in the reference state and has the same degree of hydration as revealed by thermogravimetric measurements.

First of all, we note that Bragg peak widths increase with diffraction order, and there is strong evidence that the observed widths are in effect due to a distribution of D-spacings. A direct comparison of the diffraction patterns reported in Figure 6 shows that first-order peak fwhm is almost the same for both substrates

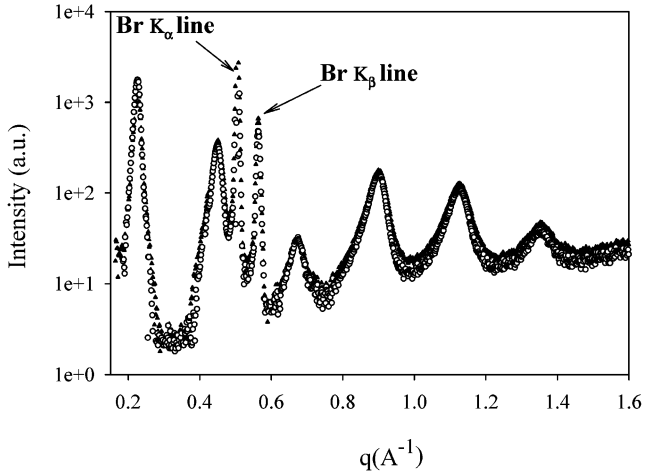

Figure 7. EDXD pattern of **1a** (open circles) and **1b** (black triangles). The diffraction intensity of **1b** is divided for clarity by a factor 1.05.

TABLE 2: FWHM of the Six Observed Orders of Diffraction of Partially Dehydrated 1a Sample Deposited on Silicon and Glass Substrate at $\theta = 2.4°$

order of reflection	fwhm (Å^{-1})	
	silicon	glass
I	0.007	0.007
II	0.025	0.030
III	0.047	0.061
IV	0.047	0.055
V	0.056	0.065
VI	0.092	0.103

whereas higher order reflections exhibit lower widths in the case of the silicon substrate (see Table 2).

This finding clearly means that the utilization of the oriented surface of silicon wafers as substrate causes a better sample orientation. From a technical point of view, these observations could also suggest that the mosaicity of the system is below the instrumental resolution. In both cases, the presence of diffuse diffraction between Bragg reflections indicates the presence of random stacking disorder. It is relevant to observe that the curve between the peaks becomes higher, the farther from the origin. Diffraction peaks represent interbilayer coherence, whereas diffuse scattering beneath them arises from diffraction lacking such coherence. In other words, this area lost from the peaks represents multibilayer-incoherent diffraction and it is lower in the case of better oriented samples. Thus, Figure 6 confirms that **1a**-supported multibilayers are better oriented when smooth silicon wafers are adopted as substrates. Indeed, the natural tendency to minimize the energy of interaction with the substrate lets the bilayer next to the surface adopt a flat configuration and maintain a fixed distance from the solid support. This configuration is more stable in the case of smooth substrates and produces a "pinning effect" that suppresses the spontaneous fluctuations of the bilayers and reduces D-spacing distribution, whereby rough surfaces weaken this effect.[23] Regardless, this difference is known to become smaller as the sample hydration is reduced and it is probably the case of the measurements of Figure 6.

Figure 7 shows the EDXD pattern of sample **1b** collected at $\theta = 2.4°$ deposited on silicon substrate compared to that of **1a**. The diffraction intensity of **1b** is divided by a factor 1.05 in order to better discriminate the diffraction patterns. It is particularly noteworthy to observe that **1a** and **1b** present the same structural features.

In Figures 6 and 7 the Br−K fluorescence lines are superimposed on the pure diffraction pattern and indicated by

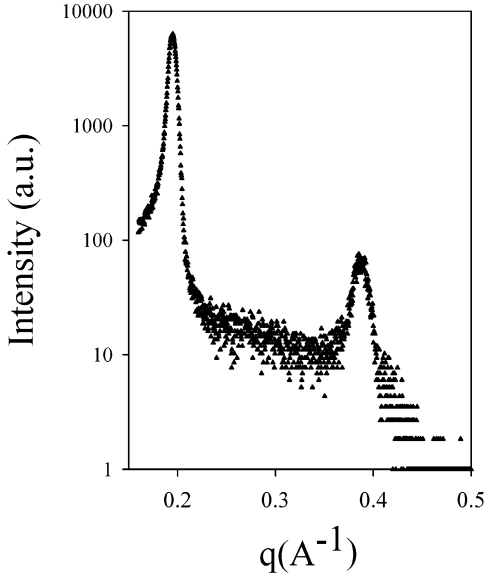

Figure 8. Diffraction pattern of fully hydrated **1c** multibilayer aligned on a silicon substrate. The diffraction angle was $\theta = 0.7°$.

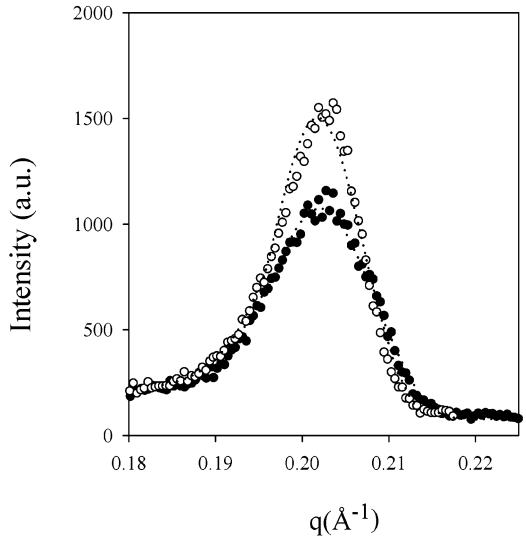

Figure 9. Comparison between the initial (black circles) and final (open circles) spectra of **1c** collected at $\theta = 0.7°$. Diffraction profiles are fitted by Gaussian distributions (dotted lines). Dehydration does not radically modify the peak position, whereas the main difference is due to the relative height of the first-order Bragg peak.

arrows. Since the fluorescence lines are produced by the de-excitation of Br atoms when ionized by the X-ray beam and each lipid molecule contains two Br atoms, it means that the intensity of the fluorescence lines depends only on the number of de-excitation events. As such, they are a useful standard that allows to check that the same amount of lipid is effectively deposited on the substrates.

To study the influence of the molecular structure on the macromolecular self-assembled morphology, the meso form **1c** was last investigated. Figure 8 depicts the first two Bragg maxima of fully hydrated **1c**, collected at $\theta = 0.7°$, which exhibit a *D*-spacing of 31.9 Å. Flowing nitrogen through the sample chamber for about 5 h caused the sample to be partly dehydrated.

A series of time-sliced diffraction patterns have been collected to follow the temporal development of the sample (40000 s). The initial and final spectra are reported in Figure 9, both fitted by a Gaussian distribution. Peak position does not remarkably

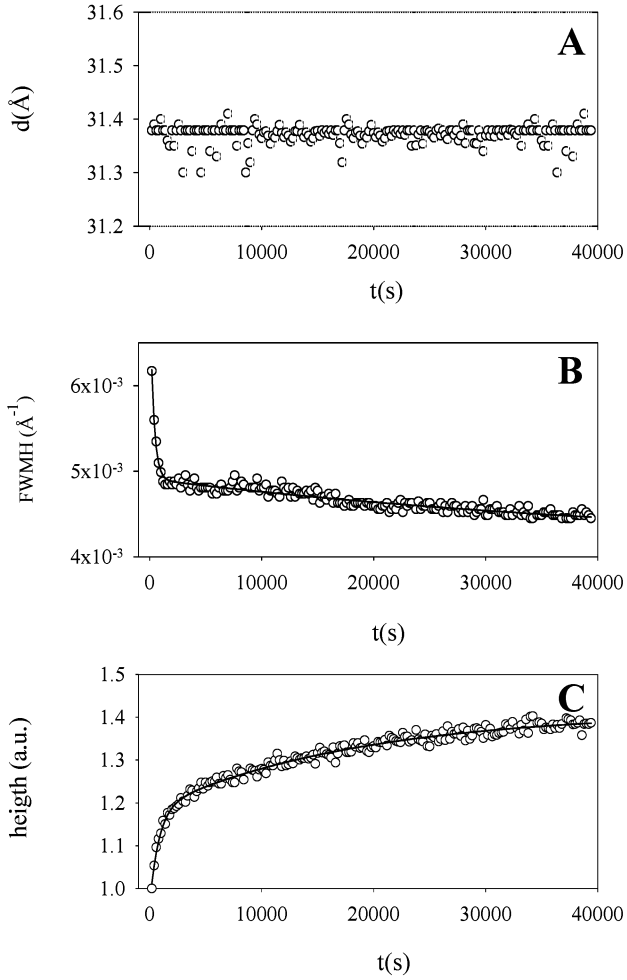

Figure 10. Temporal evolution of *D*-spacing (panel A), fwhm (panel B), height (panel C) of **1c**.

TABLE 3: Fitting Parameters of the Dehydration Kinetics of 1c Obtained Applying Eqs 2 and 4

fitting parameters	1c
σ_0 (Å^{-1})	4.11×10^{-3}
σ_1 (Å^{-1})	2.36×10^{-3}
σ_2 (Å^{-1})	8.40×10^{-4}
$\tau_{\sigma 1}$ (s^{-1})	3.26×10^{2}
$\tau_{\sigma 2}$ (s^{-1})	4.85×10^{4}
H_0 (a.u.)	1.41
H_1(a.u.)	2.4×10^{-1}
H_2 (a.u.)	2.3×10^{-1}
τ_{H1} (s^{-1})	8.12×10^{2}
τ_{H2} (s^{-1})	1.82×10^{4}

move over the entire acquisition time and the calculated *D*-spacing remains almost unchanged, implying that the sample was in a condition close to the thermodynamic equilibrium.

In the data analysis, eq 2 has been used to evaluate the temporal development of the first-order Bragg peak fwhm, whereas the following equation is used to fit the temporal profile of normalized first-order reflection height:

$$H(t) = H_0 - H_1 \exp(-t/\tau_{H1}) - H_2 \exp(-t/\tau_{H2}) \quad (H(t) \geq H_0, t \in (0, \infty)) \quad (4)$$

The results of the experiments performed are depicted in Figure 10 and listed in Table 3.

EDXD patterns of the partly dehydrated **1c** sample were collected at two diffraction angles, $\theta_1 = 0.5°$ and $\theta_2 = 2.05°$.

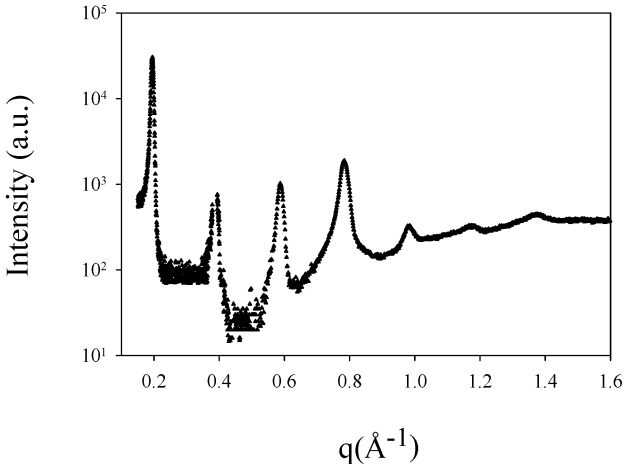

Figure 11. Diffraction pattern of partly hydrated **1c** multilayer collected at two diffraction angles ($\theta_1 = 0.5°$ and $\theta_2 = 2.05°$) and connected together. The structure resembles that of **1a** but the first-order Bragg peak is shifted to a lower q value, i.e., to a greater multilamellar D-spacing (for details see the text).

The first angle covers an overall q range from 0.095 to 0.43 Å^{-1}, whereas the latter covers the range between 0.038 and 1.6 Å^{-1}. The patterns have been connected to reconstruct the whole diffraction pattern (Figure 11).

In the spectrum, a clear maximum is located at $q = 0.202$ Å^{-1} and seven orders of diffraction are observed. The partial dehydration of the sample caused a reduction of D-spacing up to 31.4 Å and, as in the case of **1a**, sensibly improves the quality of the diffraction patterns.

All these results demonstrate that the meso form, **1c**, presents a larger value in D-spacing of about 3 Å compared to that obtained for both **1a** and **1b** samples. It is well established[17,18] that the lamellar periodicity D is the sum of the bilayer thickness d_B and thickness of the water layer d_w between opposing bilayers. The bilayer thickness is further subdivided as the sum of the steric size of the headgroup and the effective length of the hydrocarbon tails. Thermogravimetric measurements carried out on **1c** samples confirmed a number of 3.5 water molecules surrounding each surfactant unit. This finding, combined with the above-discussed effect of the partial dehydration of all the samples on the multilamellar repeat distance D, would suggest that the thickness of the thin water layer is almost the same for all the investigated samples. As a result, we believe that the observed enhancement in D-spacing observed in the meso form could not be attributed to a different hydration level. Nevertheless, it is not an unexpected result given that differences in D-spacing between diastereomeric surfactants have been previously reported.[24−26] In these studies it has been plainly shown that the headgroup conformation and its orientation with respect to the hydrophobic tails (Figure 1) control the packing properties of monomers in aqueous solutions. Indeed, diastereomeric surfactants have been found to show a different degree of chain order resulting in more folded configuration of the chains.[27] Finally, this denser packing is able to modulate the morphology and the structural properties of the aggregates.

4. Conclusions

We have characterized the structure of fully hydrated solid-supported cationic gemini **1a** multibilayers by means of energy dispersive X-ray diffraction. We observed two diffraction peaks reflecting a D-spacing of 28.4 Å. Thermogravimetric measurements reveal that, in the full hydration condition, there are 3.5 waters for **1a** molecule. Then we have studied the dehydration/hydration kinetics of **1a** sample. Our analysis of the data shows that the lipid film evolves, upon dehydration, to a partially dehydrated state, reaching a plateau over a period of about 3000 s. This more ordered state exhibits six Bragg maxima and a lower D-spacing of 27.9 Å, which remains stable over a week. Thermogravimetric measurements reveal that, in this state, there are only 1.5 water molecules for **1a** molecule. Extra-dehydrated samples evolve under the experimental conditions, coming back to the same thermodynamic equilibrium condition. We have also studied the effect of the substrate on the D-spacing of the partly dehydrated **1a** sample employing smooth silicon and rough glass supports. Even if the first-order Bragg peak position and width are the almost same, an accurate analysis of higher order reflections and of the inter-peaks diffuse scattering in the diffraction patterns shows that the mosaic spread of the system is lower when smooth silicon wafers are adopted as substrates with respect to rough glass-made supports. The chiral form **1b** presents, as expected, the same structural features. We also characterized the structure of fully hydrated **1c**, a stereoisomer of both **1a** and **1b**, which results assembled into aligned multibilayers with a D-spacing of 31.9 Å. The dehydration kinetics of **1c** was followed until the equilibrium condition was reached. Furthermore, we have shown that energy dispersive X-ray diffraction, due to its peculiar characteristics, is a suitable technique to characterize the structural features of macromolecular self-assemblies and to perform kinetic studies.

References and Notes

(1) Menger, F. M.; Keiper, J. S. *Angew. Chem., Int. Ed*. **2000**, *39*, 1906 and references therein.

(2) Kwetkat, K., Patent number WO 9731890, 1997. Dahms, G.; Kwetkat, K. DE 19943681, 2001.

(3) (a) Perez, L.; Torres, J. L.; Manrese, A.; Solans, C.; Infante, M. R. *Langmuir* **1996**, *12*, 5296. (b) Menger, F. M.; Mbadugha, N. A. *J. Am. Chem. Soc.* **2001**, *123*, 875.

(4) (a) McGregor, C.; Perrin, C.; Monck, M.; Camilleri, P.; Kirby, A. J. *J. Am. Chem. Soc.* **2001**, *123*, 6215. (b) Matti, V.; Säily, J.; Ryhänen, S. J.; Holopainen, J. M.; Borocci, S.; Mancini, G.; Kinnunen, P. *Biophys. J.* **2001**, *81*, 2135. (c) Jennings, K. H.; Marshall, I. C. B.; Wilkinson, M. J.; Kremer, A.; Kirby, A. J.; Camilleri, P. *Langmuir* **2002**, *18*, 2426. (d) Ryhänen, S. J.; Säily, M. J.; Paukku, T.; Borocci, S.; Mancini, G.; Holopainen, J. M.; Kinnunen, P. K. J. *Biophys. J.* **2003**, *84*, 578. (e) Bell, P. C.; Bergmsa, M.; Dolbnya, I. P.; Bras, W.; Stuart, M. C. A.; Rowan, A. E.; Feiters, M. C.; Engberts, J. B. F. N. *J. Am. Chem. Soc.* **2003**, *125*, 1551.

(5) (a) Luchetti, L.; Mancini, G. *Langmuir* **2000**, *16*, 161. (b) Ryhänen, S. J.; Pakkanen, A. L.; Säily, M. J.; Bello, C.; Mancini, G.; Kinnunen, P. K. J. *J. Phys. Chem. B* **2002**, *106*, 11694.

(6) (a) Zhang, Y.; Sun, P. *Tetrahedron: Asymmetry* **1996**, *7*, 3055. (b) Grassert, I.; Schiukawski, K.; Vollhardt, D.; Oehme, G. *Chirality* **1998**, *10*, 754.

(7) (a) Chlotier, J.; Tomellini, S. *J. Chromatogr. A* **1996**, *723*, 179. (b) Mechref, Y.; Elrassi, Z. *Chirality*, 1996, *8*, 518. (c) Desbene, P.; Fulchic, C. *J. Chromatogr. A* **1996**, *749*, 257. (d) Peterson, A.; Ahuja, E.; Price, R.; Nakagawa, H. *Langmuir* **1996**, *12*, 5803.

(8) (a) Arnett, E. M.; Thompson, O. *J. Am. Chem. Soc.* **1981**, *103*, 968. (b) Fuhrhop, J. H.; Schneider, P.; Rosenberg, J.; Boekema, E. *J. Am. Chem. Soc.* **1987**, *109*, 3387. (c) Jursic, B. S. *Tetrahedron Lett.* **1993**, *34*, 963. (d) Fuhrhop, J. H.; Helfrick, W. *Chem. Rev.* **1993**, *93*, 1565. (e) Stevens, F.; Dyer, D. J.; Walba, D. W. *Angew. Chem., Int. Ed. Engl.* **1996**, *35*, 900. (f) Morigaki, K.; Dalla Valle, S.; Walde, P.; Colonna, S.; Luisi, P. L. *J. Am. Chem. Soc.* **1997**, *119*, 292. (g) Belogi, G.; Croce, M.; Mancini, G. *Langmuir* **1997**, *13*, 2903. (h) Borocci, S.; Erba, M.; Mancini, G.; Scipioni, A. *Langmuir* **1998**, *14*, 1960.

(9) Maier, N. M.; Franco, P.; Lindner, W.; *J. Chromatogr. A* **2001**, *906*, 3, and references therein.

(10) Simões, S.; Slepushkin, V.; Gaspar, R.; Pedroso de Lima, M. C.; Düzgünes, N. *Gene Ther.* **1998**, *5*, 955.

(11) Safinya, C. R. *Curr. Opin. Struct. Biol*. **2001**, *11*(4), 440 and references therein.

(12) (a) Caminiti, R.; Rossi Alberini, V. *Int. Rev. Phys. Chem.* **1999**, *18*(2), 263. (b) Croce, F.; Curini, R.; Martinelli, A.; Persi, L.; Ronci, F.; Scrosati, B.; Caminiti, R. *J. Phys. Chem. B* **1999**, *103*, 48, 10632.

(13) Caracciolo, G.; Amiconi, G.; Bencivenni, L.; Boumis, G.; Caminiti, R.; Finocchiaro, E.; Maras, B.; Paolinelli, C.; Congiu Castellano, A. *Eur. Biophys. J.* **2001**, *30*, 163.

(14) Lyatskaya, Y.; Liu, Y.; Tristram-Nagle, S.; Katsaras J.; Nagle, J. F. *Phys. Rev. E* **2000**, 63, 1.

(15) Katsaras, J. *Biophys. J.* **1998**, *75*, 2157.

(16) Nagle, J. F.; Katsaras, J. *Phys. Rev. E* **1999**, *63*(6), 7018.

(17) Nagle, J. F.; Tristram-Nagle, S., *Biochim. Biophys. Acta* **2000**, *1469*, 159.

(18) Pabst, G.; Rappolt, M.; Amenitsch, H.; Laggner, P. *Phys. Rev. E* **2000**, *62*(3), 4000.

(19) Rossi Albertini, V.; Appetecchi, G. B.; Caminiti, R.; Croce, F.; Cilloco, F.; Sadun, C. *J. Macromol. Sci., Phys.* **1997**, *B 36*(5), 629.

(20) Vogel, M.; Münster, C.; Fenzl, W.; Thiaudière, D.; Salditt, T. *Phys. B* **2000**, *283*, 32.

(21) Binder, H.; Kohlstrunk, B.; Pohle, W. *J. Phys. Chem. B* **2000**, *104*, 12049.

(22) Blaubrock, A. E. *Biochim. Biophys. Acta* **1982**, *650*, 167.

(23) Tristram-Nagle, S.; Petrache, H. I.; Suter R. M.; Nagle, J. F. *Biophys. J.* **1998**, *74*, 1421 and references therein.

(24) Tickle, D.; George, A.; Jennings, K.; Camilleri, P.; Kirby, A. J., *J. Chem. Soc. Perkin Trans.* **1998**, *2*, 467.

(25) van Buuren, A. R.; Berendsen, H. J. C. *Langmuir* **1994**, *10*, 1703.

(26) Borocci, S.; Ceccacci, F.; Galantini, L.; Mancini, G.; Monti, D.; Scipioni, A.; Venanzi, M. *Chirality* **2003**, *15*, 441.

(27) Dupuy, C.; Auvray, X.; Petipas, C.; Rico-Lattes, I.; Lattes, A. *Langmuir* **1997**, *13*, 3965.